# A novel strategy to quantify the spatial resolution of X-ray tomograms featuring internal and external interfaces

Tetiana Sokoltsova[1,2], Romain Brault[2] , Peter Moonen[1,3]

[1] *Universite de Pau et des Pays de l'Adour, E2S UPPA, CNRS, DMEX, Avenue de l'Université, BP 1155, 64000, Pau, France*
[2] *Cetim Sud-Ouest, 5 rue Johannes Kepler, 64000, Pau, France*
[3] *Universite de Pau et des Pays de l'Adour, E2S UPPA, CNRS, TotalEnergies, LFCR, Avenue de l'Université, BP 1155, 64000, Pau, France*

**ABSTRACT**: X-ray computed tomography (CT) is a volumetric technique allowing to perform non-destructive morphological characterization of external and internal features of any kind of object. This property makes X-ray CT ideal for void, crack, and defect detection and for metrology applications on complex objects. A key consideration in this context is the spatial resolution of the acquired image data, that can be understood as the ability to detect fine structures and interfaces. This metric is influenced by various factors, related to both the used hardware and the acquisition protocol. Our research indicates that the spatial resolution is moreover location-dependent, even within a single acquisition. This implies that internal and external interfaces are imaged at a different spatial resolution. We developed a method to quantify this effect using a novel reference object. To illustrate the method, measurements were performed on both an industrial system and on a laboratory micro-tomograph. In addition to spatially characterizing the spatial resolution, our results allow to determine the optimal measurement parameters for a specific application requirement.

**Keywords**: X-ray tomography, image analysis, image quality, spatial resolution, MTF, reference object.

**Received** March 31, 2023; **In final form** March 31, 2023; **Published** June 2023



**Corresponding author:** Tetiana Sokoltsova, e-mail: tetiana.sokoltsova@univ-pau.fr.

## 1. INTRODUCTION

X-ray computed tomography (CT) is a powerful imaging technique having the ability to characterize the (micro-)structure of a broad variety of materials in three dimensions (3D) in a non-destructive fashion [1]–[4]. The technique is based on the physical property that X-ray radiation can travel through visually opaque objects. Hereby the X-ray beam is attenuated by the object to a degree that depends on the object's composition and density. A detector then acquires a series of projections of the object of interest at different angular positions. A reconstruction algorithm converts these angular projections into a 3D representation of the object. Herein, each voxel (i.e., three-dimensional pixel) has a grey tone that is a measure for the local linear attenuation coefficient of the material. Different materials have a different grey tone, enabling the quantitative 3D analysis of internal and external morphological features of the sample using dedicated software [5].

X-ray CT can characterise external surfaces, but also internal structures which are not accessible by conventional tactile or optical measurement systems. This is of particular importance for complex samples and additively manufactured components having internal features [6]. The technique also is widely used for quality control (pores, inclusions, cavities, weld quality, etc.) and dimensional measurements [7]. Other fields of application include the biomedical field [8], [9], geosciences [10], [11], industry [12], materials science, and the food sector [7], [13].

Image quality is of utmost importance in most applications of X-ray CT, especially when using images for dimensional assessment or quality control [7], [13], [14]. One of the key characteristics for the assessment of image quality is the spatial resolution. This metric describes the ability of the imaging system to display adjacent structures as separated entities [14]. Many parameters impact the spatial resolution [15], including the used hardware, acquisition protocol and software processing. For instance, in [16] it was shown that the spatial resolution can be significantly affected by the X-ray tube parameters (acceleration voltage and tube current) and the magnification-dependent pixel size. That study confirms that the resolution capabilities are influenced by the x-ray tube's power-dependent focal spot enlargement. In [17], the results on four CT units demonstrated that the geometrical factors, in particular pixel size and sampling distance, limit the spatial resolution. Furthermore, the number of

projections per rotation can also directly influence the image quality and consequently the spatial resolution. In addition to the acquisition strategy, the software processing imposes its limitations. For example, in [18] it was demonstrated the effect of the beam hardening artefacts, caused by the polychromaticity of the X-ray source, affects the spatial resolution.

The spatial resolution is measured in units of line pairs per mm (lp/mm), that is the amount of line pairs (pairs of black and white lines) that can be distinguished as separated within 1 mm. It means that, at high spatial frequencies, the small image structures become very difficult to resolve. Measuring the spatial resolution of a CT system is not straightforward and different approaches have been developed. Some of them are based on visual observations of a phantom with known dimensions (e.g., a JIMA pattern or a Siemens star), whereas others rely on the calculation of the modulation transfer function (MTF). The MTF of an imaging system provides a description on how the spatial frequency content of an object is transmitted by that imaging system. The advantage of using the MTF over visual examination is that it gives an objective quantifiable number, regardless of the observer, and can provide information on the imaging system's spatial resolution beyond a limiting value. It can e.g., inform about aberrations or focusing errors. The MTF can be derived from the image by analysing the sharpness at the edge of an opaque object [19], [20] or using dedicated phantoms [21]. Existing reference objects or phantoms generally address the MTF determination through external edges. However, one can question whether this metric for spatial resolution also holds for resolving embedded interfaces. Components produced by additive manufacturing can involve very complex geometries and it is all but guaranteed that the spatial resolution is a constant throughout the entire geometry. For this reason, there is a considerable interest in the characterisation of the spatial resolution of the inner features.

The current paper presents a new reference object dedicated to the evaluation of the performance of imaging systems, in particular in terms of the spatial resolution. The reference object features different internal and external diameters which makes it suitable for the characterisation of the spatial resolution of inner and outer interfaces simultaneously. In addition, the reference object allows to calculate the maximal penetration thickness, beam hardening intensities and to analyse error sources of CT for dimensional metrology, all from a single acquisition.

## 2. METHODOLOGY AND INSTRUMENTATION

To characterise the spatial resolution of a CT system, a new reference object was designed and manufactured. The reference object was employed to characterise two very different CT systems, namely an industrial tomograph and a laboratory micro-CT system. Each system covers different ranges of energies, resolutions, and sample sizes.

In this paragraph, first, the design of the reference object as well as its aim will be presented. Second, the MTF-based method for the spatial resolution calculation will be described. The last two subsections will be devoted to the presentation of the two CT systems used for validation.

### 2.1. Reference object

Designed and manufactured by Cetim Sud-Ouest [22] and the University of Pau and Pays de l'Adour [23], the reference object aims at the performance evaluation of X-ray CT systems. It is a cone made in aluminium (2017 A (AU4G)), comprised of four stacked parts (see Figure 1), each with a height of 50 mm. The top part is solid, whereas the three bottom parts integrate a central bore hole. The diameters of the internal holes are 15 mm, 35 mm, and 75 mm, respectively. The key-dimensions of the reference object are given in Figure 2.

The modular design renders the reference object versatile: individual parts can be scanned separately depending on the space constraints of the CT-system and the available source power. This enables using the same reference object for the characterisation of both an industrial system and a laboratory micro-tomograph.

The proposed object targets the characterisation of the spatial resolution of CT systems. It allows to evaluate the spatial frequency responses to internal and external interfaces of the cone at different wall thicknesses. Furthermore, with this object, other CT specificities such as the maximal penetration thickness, beam hardening intensity, and geometrical measurement errors can be determined simultaneously. However, to be able to evaluate the error sources influencing the uncertainty of CT dimensional measurements, the object should be

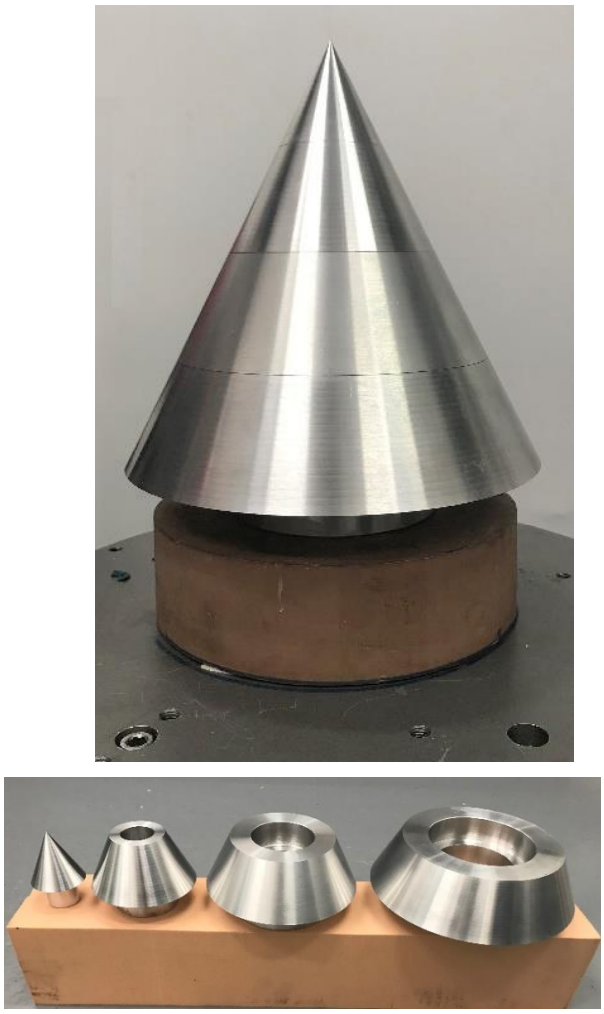

Figure 1. Picture of the assembled reference object and of its individual parts.

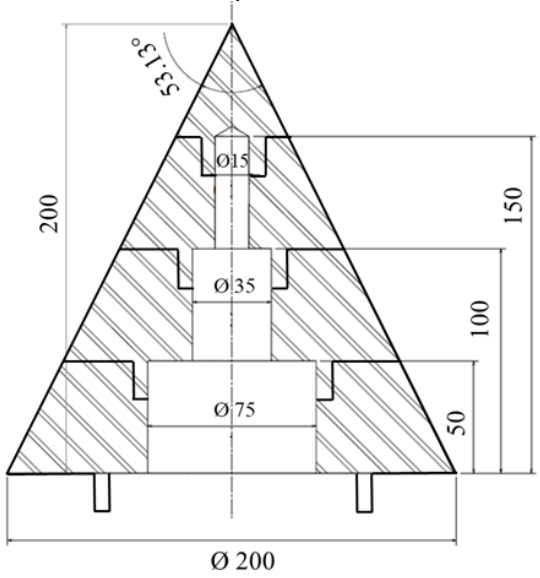


Figure 2. Technical drawing of the reference object. Length units are given in mm.

calibrated, for example by means of a tactile coordinate measuring machine (CMM).

### 2.2. Method for MTF calculation

To assess the spatial resolution of a CT system, an accurate technique to measure the MTF should be applied. In our work, we employed the edge method which is based on the measurement of edge images of an opaque object. The standard procedure consists of the following three steps: (i) first, the edge spread function (ESF) is calculated from the system response to the high contrast edge of the object; (ii) then, the derivative of the ESF yields the line spread function (LSF); (iii) and finally, taking the Fourier transform from the LSF provides the MTF. The obtained modulation profile should be normalised to 1 at zero spatial frequency.

In our method, we consider horizontal slices through the reconstructed volume of the reference object. Figure 3 (upper panel) shows a horizontal slice at 75 mm from the top of the reference object.

We employ a Hough gradient method [24] to identify the internal and external sample edges in the grey-tone image and to determine the exact centre of mass and the radii of the circular edges. A region of interest (ROI) of 50 pixels width is defined around each edge so that this encompasses the step-change in grey tone (blue and red zones in Figure 3, middle panel). The width of the ROI is identical for the inner and outer boundary to ensure that the frequency spectra will cover the same domain.

The ROIs were separated into concentric rings with a bin size of one pixel. The ESF profile is calculated by averaging the grey-tone values across each ring at the corresponding radial distance. Data averaging allows reducing the noise in the ESF profile (Figure 3, lower panel) and thus improves the signal-to-noise ratio of the MTF (Figure 4).

If applied directly, the described averaging procedure would yield much smoother MTF for the external interface than for the internal interface as the outer ROI includes a larger number of pixels. To produce compative results, each concentric *i* ring of n pixels in the outer ROI ($n_{i,\,out}$) is resampled to the number of pixels of the corresponding inner ROI ($n_{i,\,in}$). Different sampling strategies were tested, and random sampling was selected. This sampling strategy avoids interpolation errors that are inherently associated to equiangular resampling. As random sampling yields different results depending on the randomly selected data, the sampling is performed multiple times. The standard deviation of random choice of 50 iterations was estimated at 2 %.

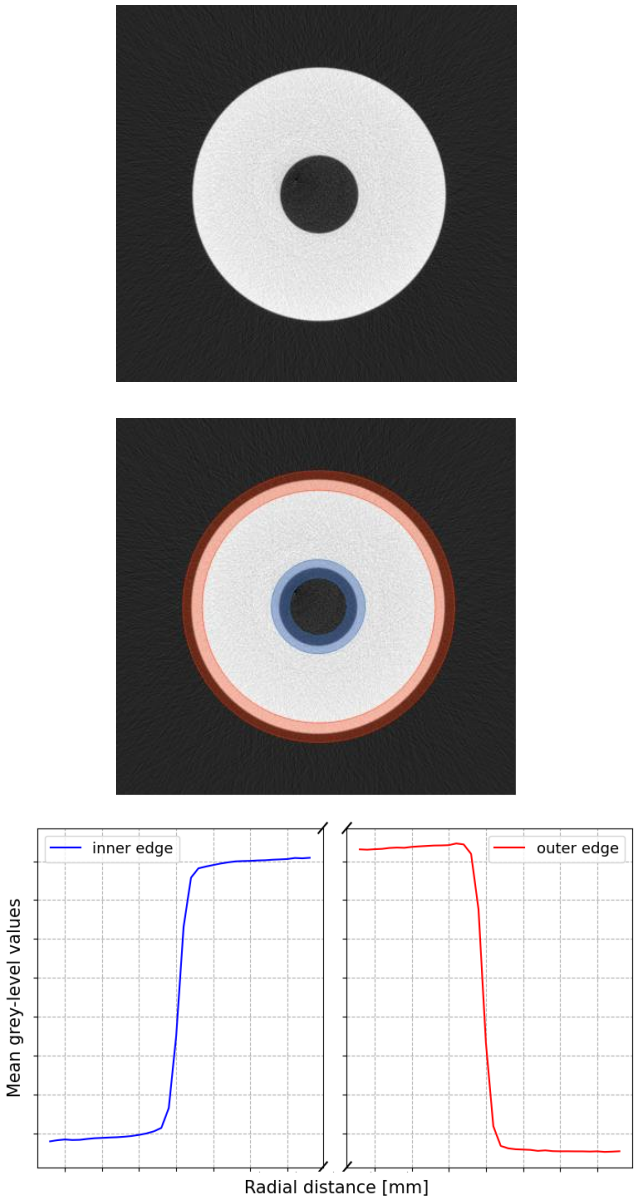


Figure 3. Horizontal slice through the reconstructed volume of the reference object (upper panel) and ROIs around the internal and external edges (middle panel). ESF profiles of both edges (lower panel).

The spatial resolution is measured as a frequency, for a given percent value of the MTF. The $MTF_{50\%}$ is defined as the spatial frequency at which the contrast falls to 50 % of the maximum value obtained at 0 lp/mm. In Figure 4, the $MTF_{50\%}$ of inner and outer edges are respectively 1.06 lp/mm and 1.15 lp/mm which correspond to 0.47 mm and 0.43 mm (in units of length).

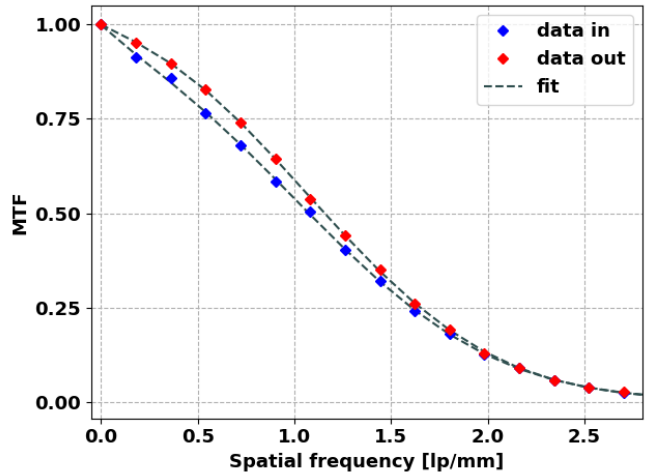


Figure 4. MTF from sharp inner and outer edges of the reference object image.

The MTF data points within both interfaces were fitted with a least square polynomial fit of fifth order, as illustrated in Figure 4.

### 2.3. Industrial CT system

The novel reference object is first used to characterize an industrial tomograph of the brand RayScan. The system consists of a fan-beam X-ray tube, a rotation stage, and a 1D linear detector (see Figure 6). The maximum distance between the source and the detector is 1.67 m. A reflection-type X-ray tube features acceleration voltages between 150 kV and 600 kV, and a maximal power of 1500 W. The detector has an 820 mm active length and 400 µm pixel pitch (i.e., 2048 pixels). The linear detector allows to minimise the scattered radiation and quickly generate a single slice image. However, in contrast to a flat panel detector, the scanning

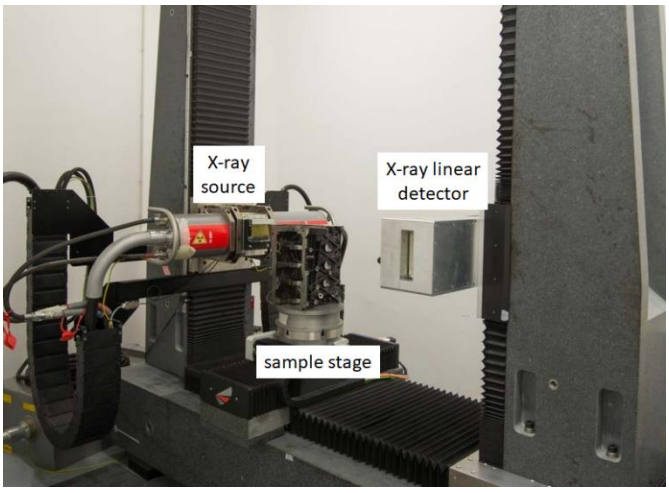


Figure 5. Industrial CT tomograph RayScan.

times for volume scans are much longer, especially when working with a tall object. The system enables to scan large-scale samples that can reach 2.5 m in height and 150 kg in weight.

### 2.4. Laboratory micro-CT system

The reference object is also used to evaluate the spatial resolution on a TESCAN UniTOM XL micro-CT system at the DMEX Centre for X-ray Imaging. The system contains a reflection-type tube, a rotation stage and a 2856 × 2856 pixel flat panel detector (see Figure 6). The microfocus tube provides a maximum power of 300 W and a tuneable energy level between 30 kVp and 180 kVp. The system allows to measure samples up to 1150 mm in height weighing up to 45 kg. The best achievable spatial resolution is 3 µm. In addition, the CT system is equipped with a spectral X-ray detector, but this one has not been characterised by means of the proposed reference object.


Figure 6. Micro-CT tomograph TESCAN.

## 3. RESULTS

The analysis compares the spatial frequency responses of both CT systems to internal and external edges of the reference object.

The two upper parts of the cone were scanned on the RayScan system (Figure 8), whereas only the top part was scanned on the TESCAN system (Figure 7) as it has a lower acceleration voltage and is therefore more limited in the material thickness which can reasonably be penetrated. The acquisition parameters of the scans are summarised in Table 1.

Thereafter, the acquired data were reconstructed with the FDK-based reconstruction algorithm, as

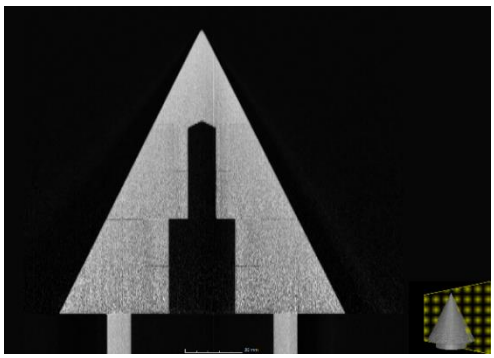

Figure 7. Vertical cut through the reconstructed volume of the reference object scanned on RayScan.

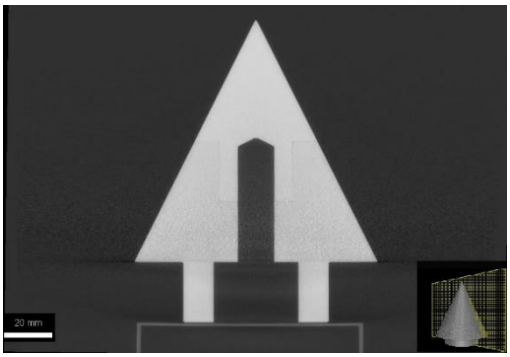


Figure 8. Vertical cut through the reconstructed volume of the reference object scanned on the TESCAN system.

implemented in software provided by RayScan Technologies and TESCAN, respectively. In our work, the characterisation of the spatial resolution is performed on the reconstructed images. Therefore, the obtained spatial resolution is affected by the reconstruction algorithm itself [18], [25]. The separate contributions of the acquisition system and the reconstruction algorithm were not singled out in the framework of the present study.

Further image analysis was performed with the help of two software packages: i) the RayScan data were treated with the commercial high-end software VGSTUDIO MAX [26], and ii) the TESCAN results with the open-source image-processing software ImageJ [27]. Any additional filters and noise smoothing were not applied to the images not to influence their quality.

Finally, the data was analysed using a custom-written code in Python (see section 2.2).

The Figure 9 and Figure 10 show the resulting MTF of both CT systems. The points represent the spatial frequency values at $MTF_{50\%}$ as a function of the penetrated wall thickness of the cone.

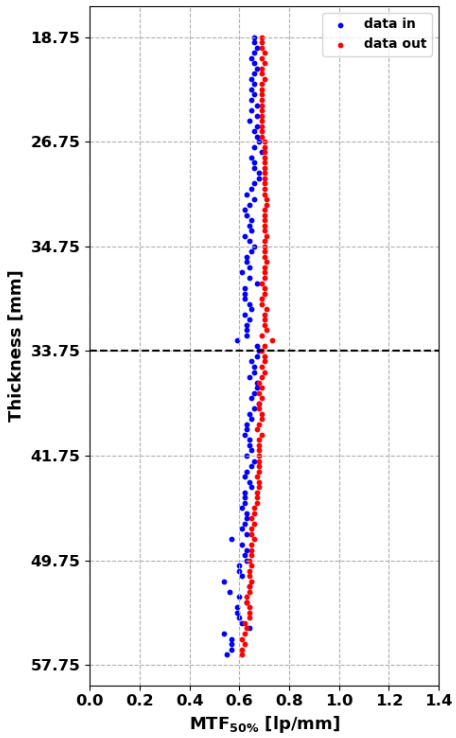


Figure 9. $MTF_{50\%}$ values within internal (blue points) and external (red point) edges as a function of the object wall thickness. The scan was performed on the RayScan system. The black dashed line indicates the junction between two parts.

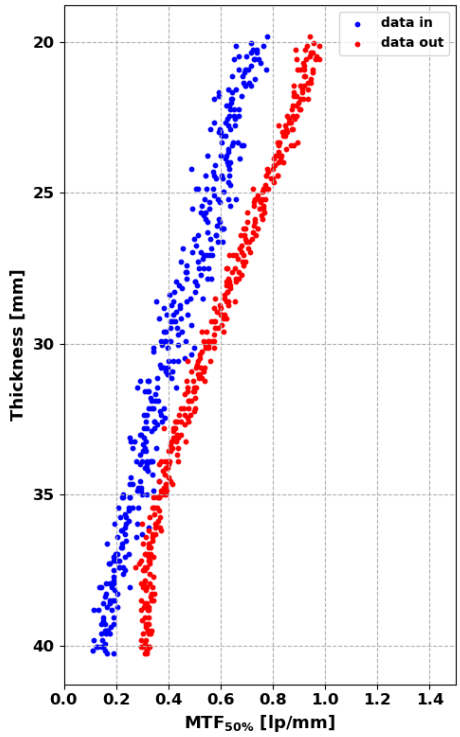


Figure 10. $MTF_{50\%}$ values within internal (blue points) and external (red point) edges as a function of the object wall thickness. The scan of the top part was performed on the TESCAN system.

## 4. DISCUSSIONS

In Figure 4, the MTF curve of the outer edge is half-Gaussian shaped, while the MTF of the inner edge is flatter, especially in the interval from 0.25 to 1. This behaviour is a result of the decreased X-ray intensity: X-rays are weakened along their path in the material, leading to a lower signal-to-noise ratio, most notably for regions closer to the centre of the object. This effect influences the image quality and, consequently, the internal interface is imaged at a lower spatial resolution compared to the external interface. Thus, the identification process of internal features could be difficult or inaccurate.

Figure 9 illustrates the $MTF_{50\%}$ values calculated from the scan of two parts of the reference object on the RayScan system. The obtained $MTF_{50\%}$ values at external and internal edges cover ranges from 0.61 lp/mm to 0.69 lp/mm and from 0.55 lp/mm to 0.67 lp/mm, respectively. The results demonstrate better MTF values from the external edge compared to the data from the internal edge which, in addition, is more widely dispersed.

For the top part of the reference object (the data plotted above the black line in Figure 9), the corresponding MTF values are roughly constant. Here, the attenuation of X-rays by the material is low and mainly affects low-energy X-ray photons. The spatial resolution at the inner interface is therefore not significantly influenced. In contrast, for the lower part of the object, the influence of the material thickness on the MTF values at the inner edge becomes more apparent due to the noise amplification in the zone closer to the internal edge. Moreover, the MTF values at the outer edge decrease with an increase in the outer diameter of

Table 1. CT scanning protocols on two systems.

| Parameter | RayScan CT | TESCAN CT |
|---|---|---|
| Voltage / kV | 450 | 150 |
| Power / W | 540 | 110 |
| Acquisition time | 12h50 | 52 min |
| Magnification | 3.93 | 2.73 |
| Voxel size / µm | 101.85 | 110 |
| Number of projections | 1170 | 2142 |
| Filter | Cu 2 mm | Sn 1.75 mm |

the object. This could be caused by the broadened X-ray beam penumbra.

Figure 10 shows the $MTF_{50\%}$ data from measurements of the top part of the reference object performed on the TESCAN system. The MTF values cover a range from 0.30 lp/mm to 0.96 lp/mm and from 0.12 lp/mm to 0.76 lp/mm, respectively, at external and internal edges. The obtained values show the same behaviour at the RayScan data. The spatial resolution at the outer edge is higher than that at the inner edge. For greater wall thicknesses, the radiation intensities are insufficient to achieve satisfactory signal-to-noise ratios.

## 5. CONCLUSIONS

In this work, we presented a modular conical reference object, particularly dedicated to the spatial resolution assessment. The obtained results in this work emphasize the difference between the spatial resolution of the inner and outer interfaces. The results from the industrial system RayScan and laboratory micro-tomograph TESCAN demonstrated that the MTF values at the internal interface are worse and more widely dispersed with increasing wall thickness when compared to the MTF values of the external interface. This is the consequence of the increased X-ray attenuation with increasing wall thickness.

Our work let us to conclude that the MTFs of inner and outer edges differ due to the noise amplification in the zone closer to the internal edge. The MTF of the inner interface is limited by the material thickness and the applied tube power. Finally, our results enabled to better predict the achievable spatial resolution of internal and external features of both imaging systems depending on the material thickness penetrated by the X-rays.

In addition, the presented reference object can be used for the assessment of other metrics for image quality characterisation and correction of CT measurement errors.

## ACKNOWLEDGEMENT

We acknowledge the ASN (under grant number ANR-21-PRRD-0059-01) and Cetim Sud-Ouest for financial support of this research. We thank UPPA's APLILAP and notably Laurent Marlin for support in the design and realisation of the reference object. We are also very grateful to Benoit Rodrigues and Ximun Lambert from Cetim Sud-Ouest and Stephan Faucher from DMEX for their valuable advice and support on X-ray CT acquisitions.

## REFERENCES

[1] P. J. Withers *et al.*, X-ray computed tomography, Nature Reviews Methods Primers, 1, 1-21 (2021), https://doi.org/10.1038/ s43586-021-00015-4.

[2] W. A. Kalender, X-ray computed tomography, Physics in Medicine and Biology, 51, R29-R43, (2006), https://doi.org/10.1088/0031-9155/51/13/R03.

[3] A. Cantatore, P. Müller, Introduction to computed tomography, DTU Mechanical Engineering, Kgs.Lyngby (2011).

[4] H. Villarraga-Gómez, Seeing is believing: X-ray computed tomography for quality control, Quality Magazine, 55, 20-23 (2016).

[5] J. Kastner and C. Heinzl, X-ray computed tomography for non-destructive testing and materials characterization, in: Integrated Imaging and Vision Techniquesfor Industrial Inspection, Springer-Verlag London Ltd, 227-250 (2015), https://doi.org/10.1007/978-1-4471-6741-9_8.

[6] A. Townsend, N. Senin, L. Blunt, R. K. Leach, and J. S. Taylor, Surface texture metrology for metal additive manufacturing: a review, Precis. Eng. 46, 34–47 (2016), https://doi.org/10.1016/j.cirp.2011.05.006.

[7] J. P. Kruth, M. Bartscher, S. Carmignato, R. Schmitt, L. De Chiffre, and A. Weckenmann, Computed tomography for dimensional metrology, CIRP Ann. Manuf. Technol. 60, 821–842 (2011), https://doi.org/10.1016/j.cirp.2011.05.006.

[8] C. M. C. Tempany, B. J. McNeil, Advances in Biomedical Imaging, JAMA, 285, 562–567 (2001), https://doi.org/10.1001/jama.285.5.562.

[9] G. Probst, B. Boeckmans, W. Dewulf, and J.-P. Kruth, Computed tomography: a powerful imaging technique in the fields of dimensional metrology and quality control, SPIE Commercial + Scientific Sensing and Imaging, 9868, Baltimore, USA (2016), https://doi.org/10.1117/12.2227146.

[10] V. Cnudde and M. N. Boone, High-resolution X-ray computed tomography in geosciences: a review of the current technology and applications, Earth-Science Reviews, 123,

1–17 (2013), https://doi.org/10.1016/j.earscirev.2013.04.003.

[11] F. Mees, R. Swennen, M. Van Geet, & P. Jacobs, Applications of X-ray computed tomography in the geosciences, Geological Society, 1–6 (2003), https://doi.org/10.1144/GSL.SP.2003.215.01.01.

[12] L. De Chiffre, S. Carmignato, J. P. Kruth, R. Schmitt, and A. Weckenmann, Industrial applications of computed tomography, CIRP Ann. Manuf. Technol., 63, 655–677 (2014), http://dx.doi.org/10.1016/j.cirp.2014.05.011.

[13] A. Singhal, J. C. Grande, and Y. Zhou, Micro/Nano-CT for Visualization of Internal Structures, Microscopy Today, 21, 16–22 (2013), https://doi.org/10.1017/S1551929513000035.

[14] W. A. Kalender, Image quality, in: Computed Tomography: Fundamentals, System Technology, Image Quality, Applications, 3th edn, Wiley-VCH, Erlangen, 111-174, (2011).

[15] VDI/VDE 2630-1.2 (2018) Computed Tomography in Dimensional Measurement—Influencing Variables on Measurement Results and Recommendations for Computed Tomography Dimensional Measurements (2018).

[16] J. Rueckel, M. Stockmar, F. Pfeiffer, and J. Herzen, Spatial resolution characterization of a X-ray micro CT system, Applied Radiation and Isotopes, 94, 230–234 (2014), http://dx.doi.org/10.1016/j.apradiso.2014.08.014.

[17] M. V Yester and G. T. Barnes, The geometrical limitation of computed tomography scanner resolution, Optical Instrumentation in Medicine VI, Boston, USA, 296-303 (1977), https://doi.org/10.1117/12.955953.

[18] E. Van de Casteele, D. Van Dyck, J. Sijbers, and E. Raman, The effect of beam hardening on resolution in x-ray microtomography, Medical Imaging 2004: Image Processing, California, USA, 2089-2096 (2004), https://doi.org/10.1117/12.535263.

[19] ISO 15708-3: Essais non destructifs-Méthodes par rayonnements pour la tomographie informatisée - Partie 3: Fonctionnement et interprétation (2017).

[20] ASTM E1695-95, Standard Test Method for Measurement of Computed Tomography (CT) System Performance (2013).

[21] S. N. Friedman, G. S. K. Fung, J. H. Siewerdsen, and B. M. W. Tsui, A simple approach to measure computed tomography (CT) modulation transfer function (MTF) and noise-power spectrum (NPS) using the American College of Radiology (ACR) accreditation phantom, Med. Phys. 40, 051907 (2013), https://doi.org/10.1118/1.4800795.

[22] Centre d'expertise Leader de la Métrologie - Cetim Sud-Ouest, https://www.cetimsudouest.fr (accessed Feb. 13, 2023).

[23] DMEX: the Centre for X-ray Imaging, https://imagingcenter.univ-pau.fr/index.php?lan=en (accessed Mar. 08, 2023).

[24] E. R. Davies, The Hough transform and its nature, in: Machine Vision Theory, Algorithms, Practicalities Signal Processing and its Applications, 3th edn, 315-337 (2005).

[25] C. Anam, F. Haryanto, I. Arif, and G. Dougherty, An investigation of spatial resolution and noise in reconstructed CT images using iterative reconstruction (IR) and filtered back-projection (FBP), Conf. Series: Journal of Physics, 1127, 1-6(2019), https://doi.org/10.1088/1742-6596/1127/1/012016.

[26] Volume Graphics, VG Studio MAX-User Mannual–3.4. 2020.

[27] C. A. Schneider, W. S. Rasband, and K. W. Eliceiri, NIH Image to ImageJ: 25 years of image analysis, Nat Methods, 9, 671–675 (2012), https://doi.org/10.1038/nmeth.2089.